

Supplementary information

Interactions of tropical cyclones with global energy and water cycles

**In the format provided by
the authors and unedited**

Supplementary Material for

Interactions of tropical cyclones with global energy and water cycles

Zhanhong Ma^{1†}, Lijing Cheng^{2†}, Suzana J. Camargo^{3,4}, Kevin E. Trenberth^{5,6}, I. I. Lin⁷, Gregory R. Foltz⁸, Daniel R. Chavas⁹, Deyuan Zhang¹, Elizabeth A. Ritchie^{10,11}, Jianfang Fei¹, Claudia Pasquero¹², Kevin J. E. Walsh¹³, Zheming Tan¹⁴, Ryan L. Sriver¹⁵, Hexin Ye¹, and Lei Zhou¹⁶

¹ College of Meteorology and Oceanography, National University of Defense Technology, Changsha, China

² State Key Laboratory of Earth System Numerical Modeling and Application, Institute of Atmospheric Physics, Chinese Academy of Sciences, Beijing, China

³ Lamont-Doherty Earth Observatory, Columbia University, Palisades, NY, USA

⁴ Columbia Climate School, Columbia University, New York, NY, USA

⁵ National Center for Atmospheric Research, Boulder, CO, USA

⁶ Department of Physics, University of Auckland, Auckland, New Zealand

⁷ Department of Atmospheric Sciences, National Taiwan University, Taipei, Taiwan

⁸ Atlantic Oceanographic and Meteorological Laboratory, NOAA, Miami, FL, USA

⁹ Department of Earth, Atmospheric and Planetary Sciences, Purdue University, West Lafayette, Indiana, USA

¹⁰ School of Earth, Atmosphere & Environment, Monash University, Clayton, VIC, Australia

¹¹ The Australian Research Council Centre of Excellence for Weather of the 21st Century, Monash University, Clayton, VIC, Australia

¹² Department of Earth and Environmental Sciences, Università di Milano-Bicocca, Milan, Italy

¹³ School of Geography, Earth and Atmospheric Sciences, University of Melbourne, Melbourne, Victoria, Australia

¹⁴ School of Atmospheric Sciences, Nanjing University, Nanjing, China

¹⁵ Department of Climate, Meteorology & Atmospheric Sciences, University of Illinois at Urbana–Champaign, Urbana, Illinois, USA

¹⁶ State Key Laboratory of Submarine Geoscience and School of Oceanography, Shanghai Jiao Tong University, Shanghai, China

†e-mail Zhanhong Ma: mazhanhong17@nudt.edu.cn; Lijing Cheng: chenglij@mail.iap.ac.cn

Supplementary Note 1 | Details of Fig. 2

Spatial and latitudinal distributions of tropical cyclone (TC)-induced surface enthalpy fluxes, loss of kinetic energy, and TC rainfall. They are calculated using an objective tracking and compositing method. First, 6-h TC center positions are identified using the IBTrACS¹⁰ best track data. For each data sample, an area with a 500-km radius from the center is defined, with a time window spanning -3 h to +3 h. The 6-h accumulated surface fluxes, kinetic energy loss, and rainfall are calculated within this area. All global TCs are then spatially summed and annually averaged to obtain the spatial distribution of annually accumulated TC contribution. A meridional integration is performed to obtain the latitudinal distributions of each term, with the percentages quantified from their latitudinal profiles divided by the corresponding climatological mean.

Supplementary Note 2 | Details of key numbers in Figs. 3 and 5

TC rainfall. Both the Global Precipitation Measurement (GPM¹; 2001-2020; 0.1°×0.1°) and Tropical Rainfall Measuring Mission (TRMM²; 1998-2019; 0.25°×0.25°) satellite precipitation products at 3-h intervals are used to calculate the tropical cyclone (TC) rain and global rain. A radius of 500 km is used to define the TC rainfall area as in previous studies^{3,4}. The averaged annually accumulated TC rainfall is 15.6×10^{15} kg y⁻¹ and 12.5×10^{15} kg y⁻¹ for GPM and TRMM, respectively. The heat transport from the TC rainfall is estimated at 0.58 PW (Ref.⁵), which is equivalent to 7.3×10^{15} kg y⁻¹ (1 PW = 12.6×10^{15} kg y⁻¹). Therefore, the TC rainfall is estimated in the range of 7.3 - 15.6×10^{15} kg y⁻¹.

Evaporation under TCs. The annual mean surface enthalpy flux was estimated at 0.17 PW (Ref.⁵). Given that surface latent heat flux constitutes approximately 90% of surface enthalpy flux, the surface latent heat flux is estimated at 0.15 PW, corresponding to 1.9×10^{15} kg y⁻¹. The modeled surface latent heat flux by the reconstructed wind fields (Ref.⁶) is 0.22 PW, corresponding to 2.8×10^{15} kg y⁻¹. The annual surface evaporation under TCs is estimated in the range of 1.9 - 2.8×10^{15} kg y⁻¹.

Moisture convergence. According to previous water budgets of TCs, surface evaporation accounts for 10%-30% of total water loss of TCs, with the moisture convergence roughly accounting for the other part (70%-90%; Ref.^{5,7,8}). This fraction is applied to the rain range of 7.3 - 15.6×10^{15} kg y⁻¹ to derive the lower and upper bounds of moisture convergence: 5.1 - 14×10^{15} kg y⁻¹.

LHR (energy conversion). The TC rain is used to obtain the accumulated latent heat release of the TC system. The GPM and TRMM estimations of 15.6×10^{15} kg y⁻¹ and 12.5×10^{15} kg y⁻¹ correspond to 1.2 PW and 0.99 PW, respectively. The model-based empirical relationships give an estimate of rainfall by 0.58 PW (Ref.⁵). The annual mean LHR is thus estimated in the range of 0.58-1.2 PW.

Surface enthalpy flux decreases over cold wakes. The anomalously downward heat flux at the air-sea interface drives the cold wake recovery, representing a restoration of energy by the ocean from the atmosphere⁹. The total amount of surface enthalpy flux decrease is equal to the sum of the surface enthalpy flux during TCs and the ocean heat uptake (OHU) left by TCs. The surface enthalpy flux during TCs is in the range of 0.17-

0.25 PW, and the OHU is in the range of 0.13-1.4 PW. A sum of these two terms gives a value range of 0.3-1.65 PW.

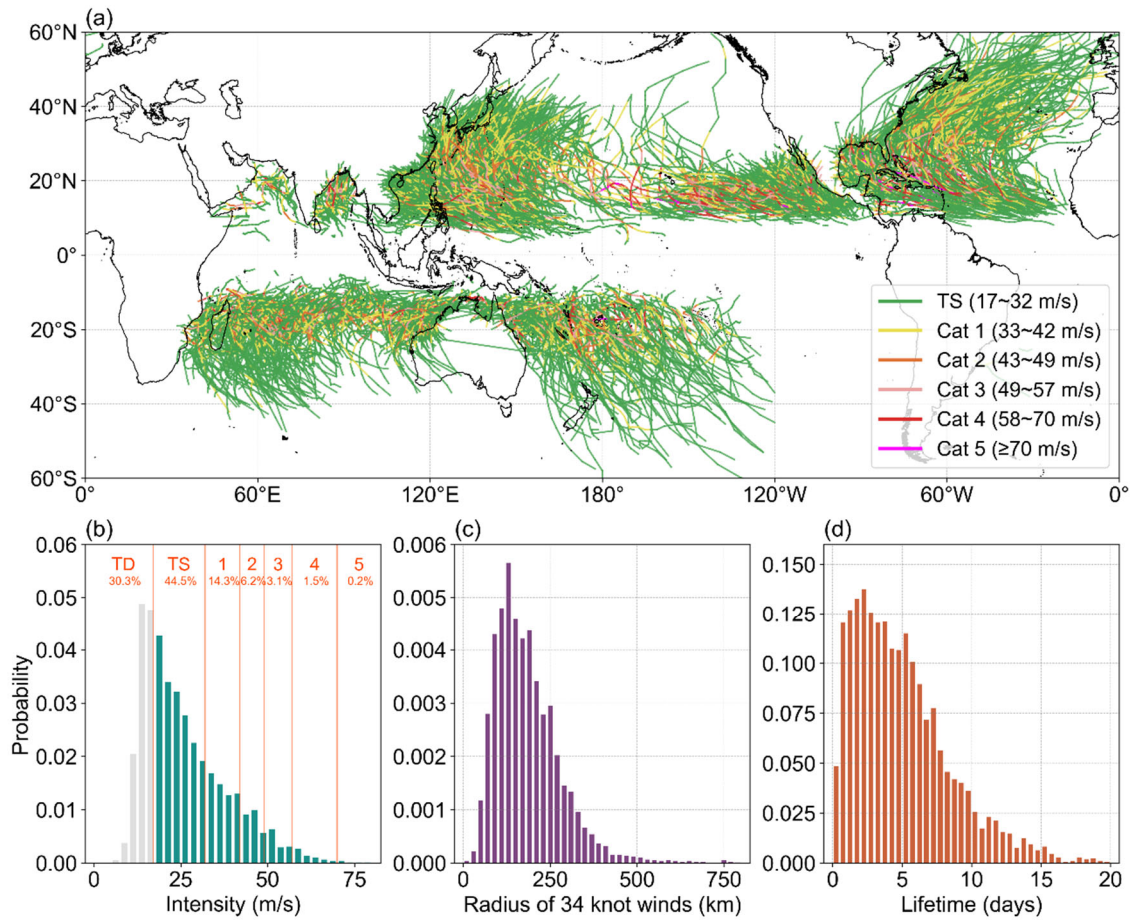
Surface evaporation decreases over cold wakes. The annual mean surface evaporation over cold wakes, equivalent to surface latent heat flux, is estimated at 0.27-1.49 PW (90% of surface enthalpy flux decreases), corresponding to $3.4\text{-}18.7 \times 10^{15}$ kg y^{-1} .

Supplementary Note 3 | Details of Fig. 4d

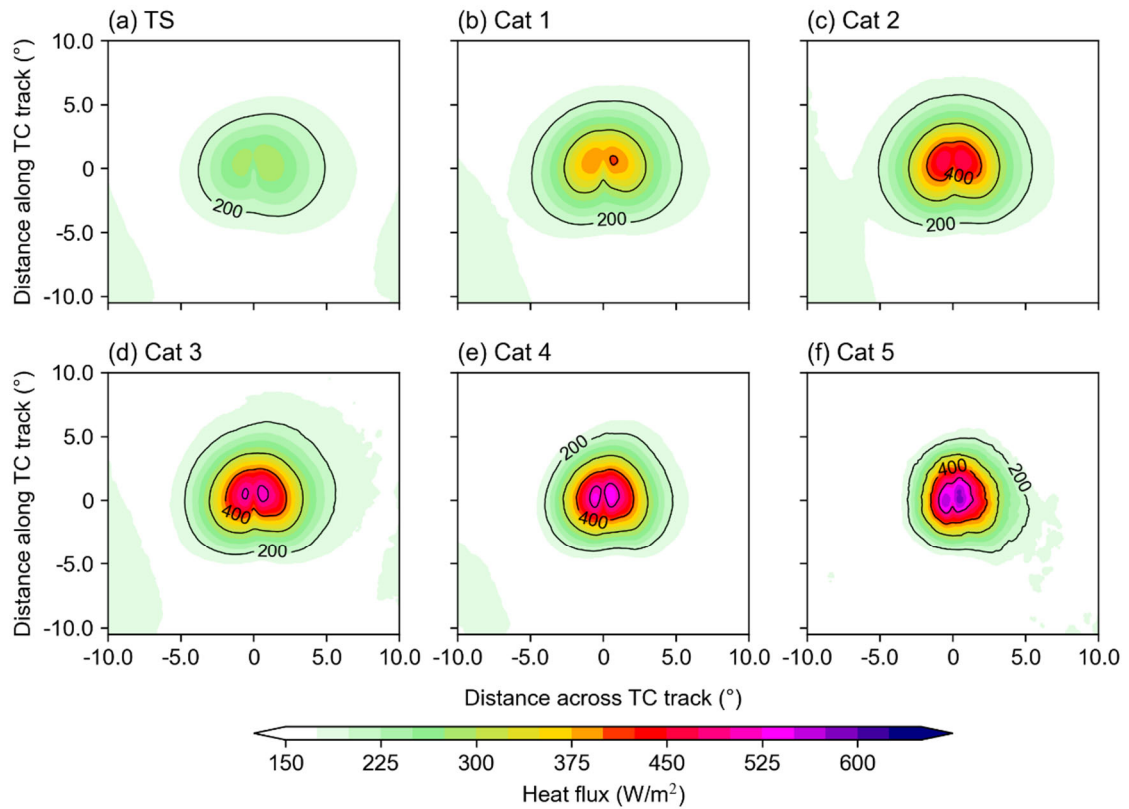
Moist static energy anomalies. The time-height evolution of moist static energy anomalies is obtained using ERA5 reanalysis data¹¹ from 1998 to 2022, combined with TC best track data from IBTrACS. The analysis focused on land-falling TCs that persisted over land for at least 24 hours. Moist static energy is defined as:

$$\text{MSE} = c_p T + gz + L_v q,$$

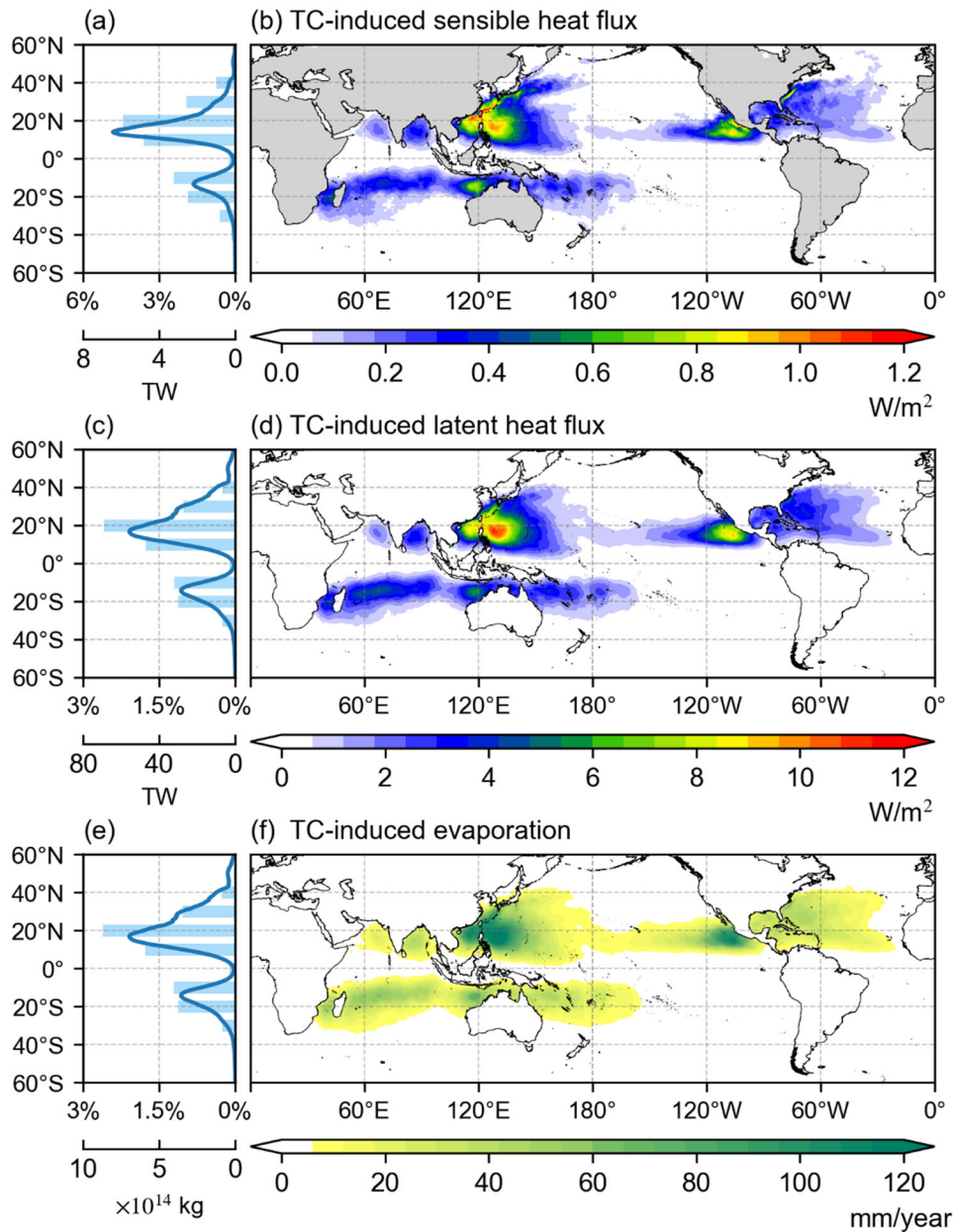
where MSE is moist static energy, c_p is specific heat at constant pressure, T is air temperature, g is gravitational acceleration, z is geopotential height, L_v is latent heat of vaporization, and q is specific humidity. For each 6-h TC data sample, an area average is computed over a $5^\circ \times 5^\circ$ domain centered on the TC center. The temporal evolution is calculated with a time window ranging from 10 days before to 30 days after the passage of a TC. Moist static energy anomalies are then obtained by removing the multiyear climatological mean.



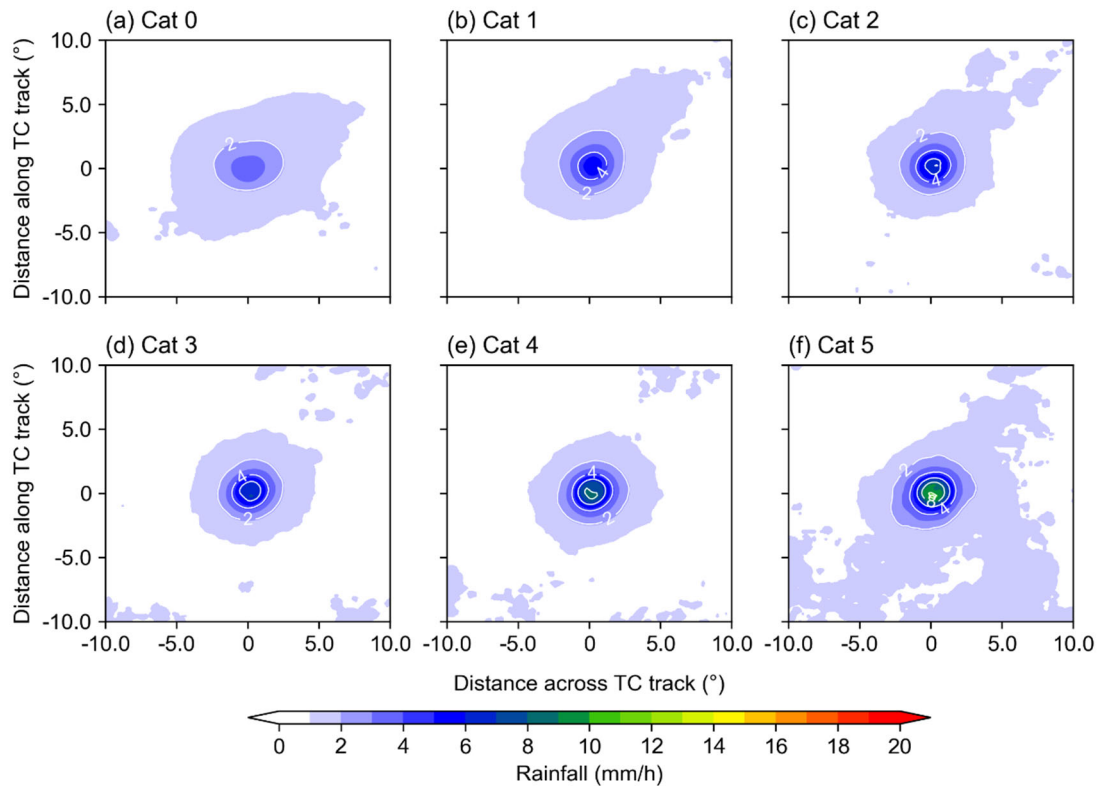
Supplementary Figure 1 | TC characteristics. (a) Spatial distributions of global TC tracks and Saffir-Simpson intensities. PDFs of (b) TC intensity (maximum surface wind), (c) TC size (radius of 34-knot winds), and (d) TC lifetimes. TC records are from best track data of the official World Meteorological Organization (WMO) agency in International Best Track Archive for Climate Stewardship (IBTrACS¹⁰, version 4), during 1980-2022.



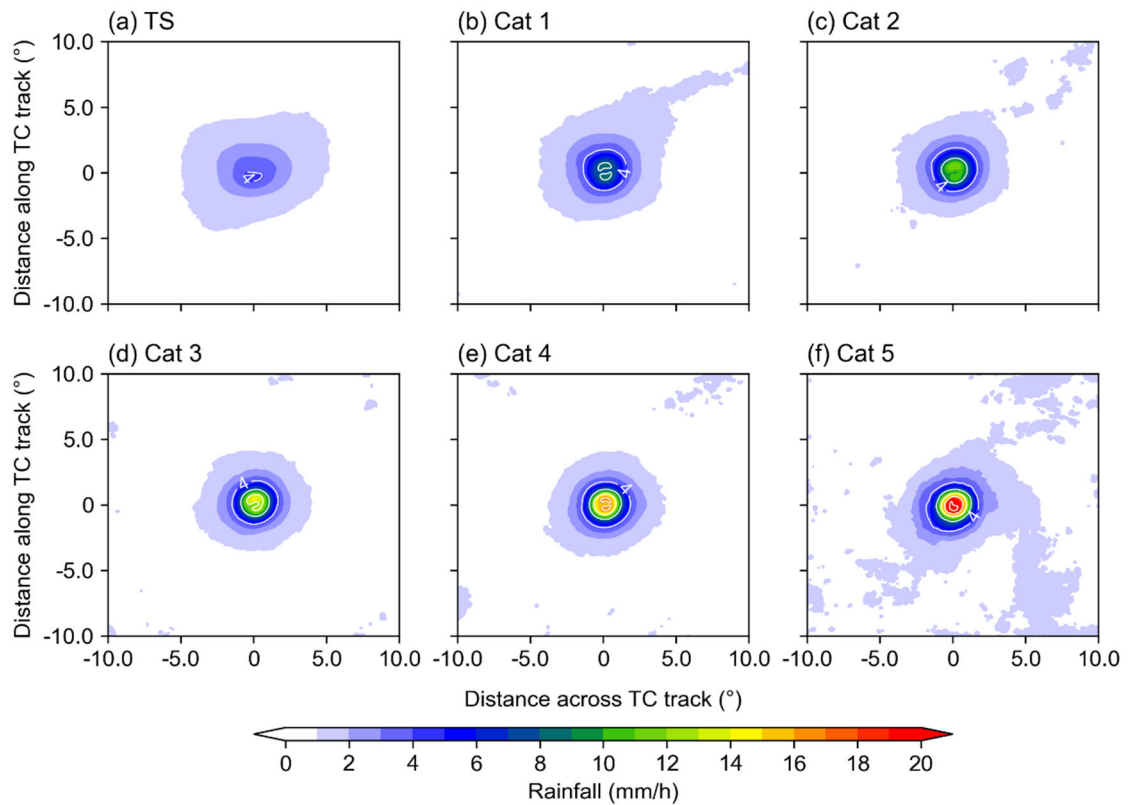
Supplementary Figure 2 | Typical magnitudes of surface enthalpy flux under TCs. Plan views of composite surface enthalpy flux during 1993-2016, classified according to the Saffir-Simpson category for (a) tropical storm, (b) Cat 1, (c) Cat 2, (d) Cat 3, (e) Cat 4, and (f) Cat 5. Calculation is conducted based on model data in Ref.⁶.



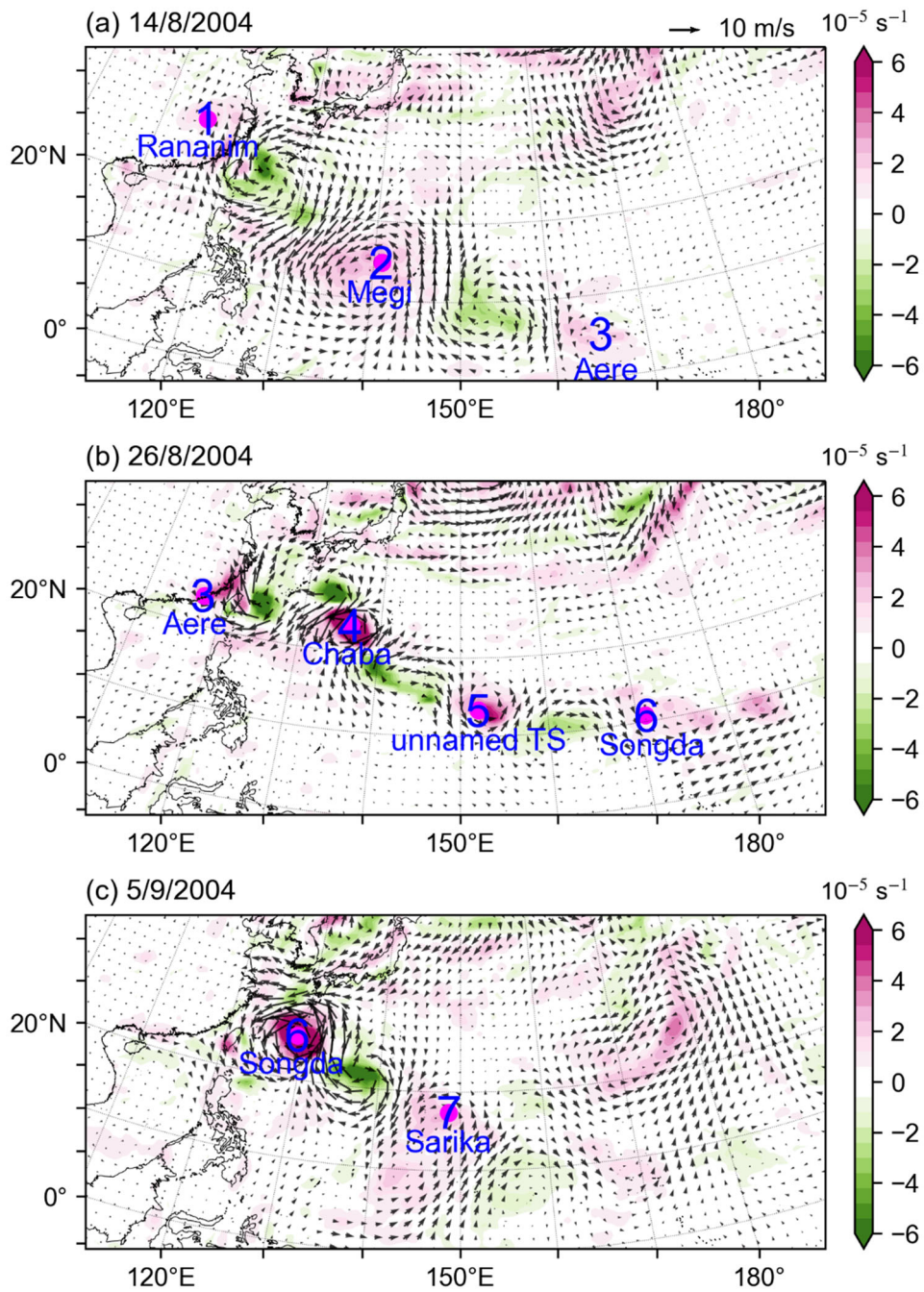
Supplementary Figure 3 | Surface sensible and latent heat flux and surface evaporation of TCs. Spatial distributions of annually averaged TC-induced (a) surface sensible heat flux, (b) surface latent heat flux and (c) surface evaporation induced by TCs. Note that (b) is equivalent to (c) but with different units. Calculation is conducted based on model data in Ref.⁶.



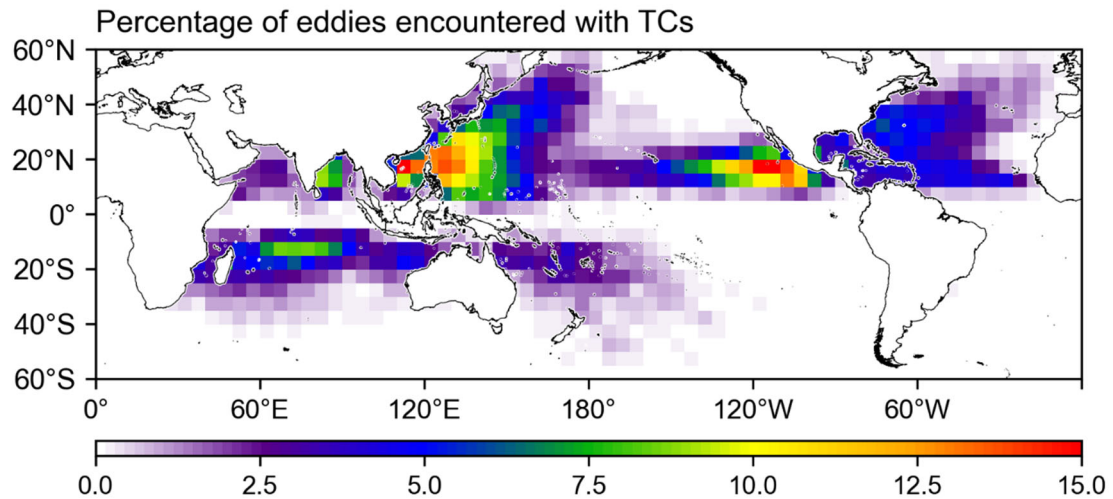
Supplementary Figure 4 | Typical magnitudes of TC rain rates based on TRMM² dataset. Plan views of composite TC rain rates from 1998 to 2019, classified according to the Saffir-Simpson category for (a) Cat 0 (tropical storm), (b) Cat 1, (c) Cat 2, (d) Cat 3, (e) Cat 4, and (f) Cat 5. Contours are at intervals of 1 mm h⁻¹.



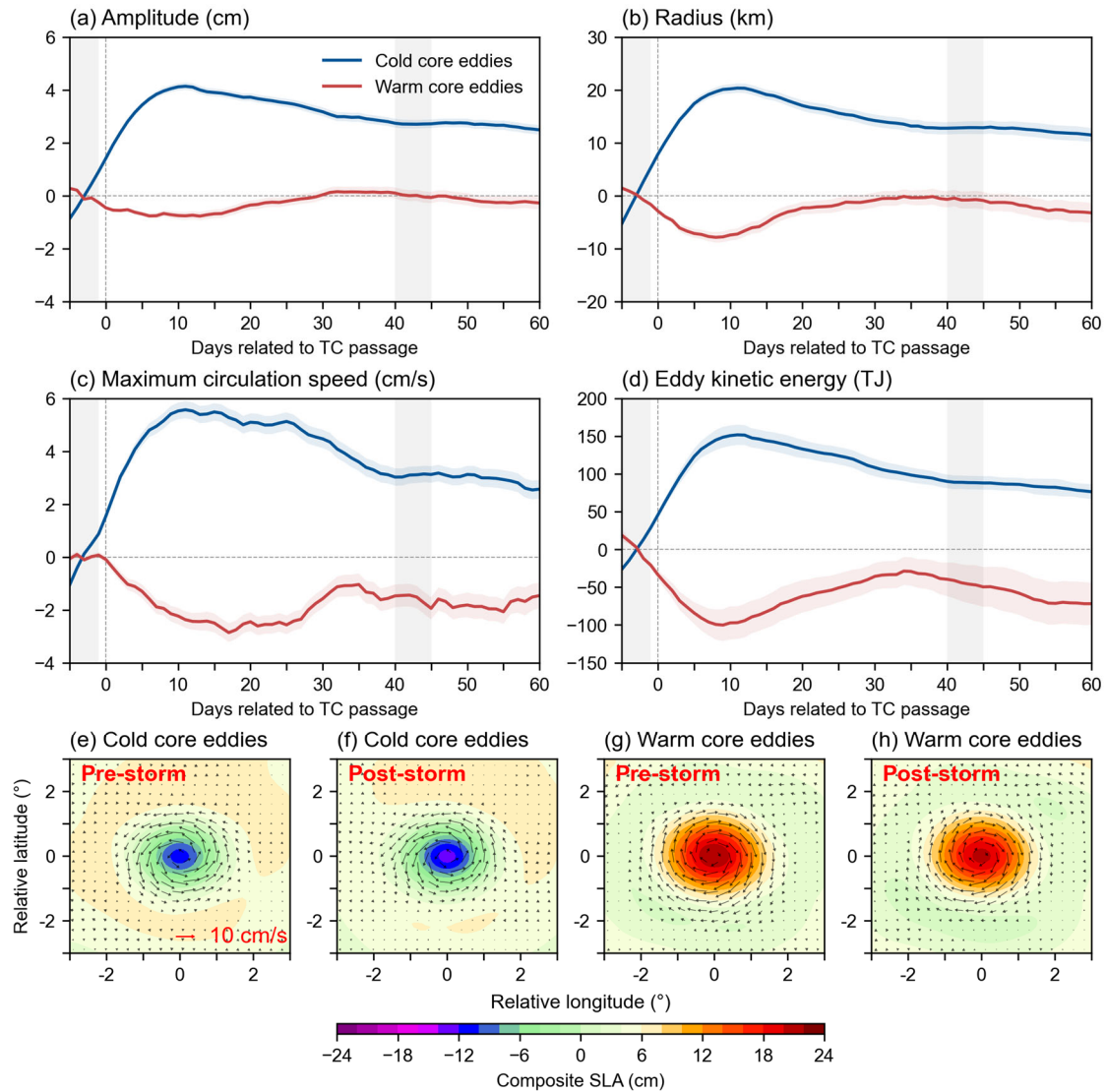
Supplementary Figure 5 | Typical magnitudes of TC rain rates based on GPM¹ dataset. Plan views of composite TC rain rates from 1998 to 2019, classified according to the Saffir-Simpson category for (a) Cat 0, (b) Cat 1, (c) Cat 2, (d) Cat 3, (e) Cat 4, and (f) Cat 5. Contours are at intervals of 1 mm h⁻¹.



Supplementary Figure 6 | Multiple tropical cyclogenesis events over the western North Pacific. The 3- to 8-day filtered surface wind (vector) and relative vorticity fields (shaded) on (a) August 14th 2004, (b) August 26th 2004, and (c) September 5th 2004 (replotted from data in Ref.¹²).



Supplementary Figure 7 | Percentages of mesoscale oceanic eddies encountered by TCs. Spatial distributions of percentages (%) of mesoscale oceanic eddies interacted with TCs in 5°×5° bins over 1993-2020. Eddy information is from the delayed-time version 3.2 release of the Mesoscale Eddy Trajectory Atlas product¹³. TC records are from best track data of the official WMO agency in IBTrACS¹⁰ version 4. The TC-eddy interaction is defined to occur as their central distance is equal to or smaller than the eddy radius¹⁴.



Supplementary Figure 8 | Impact of TCs on Mesoscale Oceanic Eddies. Temporal evolution of TC-induced anomalies in (a) amplitude (cm), (b) radius (km), (c) maximum circulation speed (cm/s), and (d) integrated eddy kinetic energy (TJ) for cold core eddies (blue) and warm core eddies (red), relative to the pre-storm period (averaged -5 to -1 days before TC passage). Shading indicates standard errors. Composite sea level anomaly (shaded; cm) and geostrophic currents (vector; cm s^{-1}) for (e),(f) cold core eddies and (g),(h) warm core eddies during the (e),(g) pre-storm (averaged days -5 to -1) and (f),(h) post-storm (averaged days +40 to +45) periods. The locations of mesoscale ocean eddies were obtained from the delayed-time version 3.2 release of the META3.2 (Ref.¹⁵) product. Eddy amplitude, radius, and maximum circulation speed in (a)-(c) are calculated from the composite sea level anomaly map of AVISO¹⁶ product using the method of Ref.¹³. The eddy kinetic energy in (d) is calculated using a two-layer reduced gravity model with vertical profiles derived from WOA¹⁷ seasonal data, as described in Ref.¹⁸. The composite analysis spans the period from 1993 to 2020.

References

1. Huffman, G. J. *et al.* Integrated Multi-satellite Retrievals for the Global Precipitation Measurement (GPM) Mission (IMERG). in *Satellite Precipitation Measurement* (eds Levizzani, V. et al.) vol. 67 343–353 (Springer International Publishing, Cham, 2020).
2. Huffman, G. J. *et al.* The TRMM Multisatellite Precipitation Analysis (TMPA): Quasi-global, multiyear, combined-sensor precipitation estimates at fine scales. *J. Hydrometeorol.* **8**, 38–55 (2007).
3. Guzman, O. & Jiang, H. Global increase in tropical cyclone rain rate. *Nat. Commun.* **12**, 5344 (2021).
4. Ma, Z. *et al.* Strengthening cold wakes lead to decreasing trend of tropical cyclone rainfall rates relative to background environmental rainfall rates. *npj Clim. Atmos. Sci.* **6**, 131 (2023).
5. Trenberth, K. E. & Fasullo, J. Water and energy budgets of hurricanes and implications for climate change. *J. Geophys. Res.* **112**, 2006JD008304 (2007).
6. Zhang, D. *et al.* Oceanic memory of tropical cyclones moderates the Kuroshio current. *Nat. Commun.* **16**, 6890 (2025).
7. Yang, M.-J., Braun, S. A. & Chen, D.-S. Water budget of Typhoon Nari (2001). *Mon. Weather Rev.* **139**, 3809–3828 (2011).
8. Trenberth, K. E., Davis, C. A. & Fasullo, J. Water and energy budgets of hurricanes: Case studies of Ivan and Katrina. *J. Geophys. Res.* **112**, 2006JD008303 (2007).
9. Emanuel, K. Contribution of tropical cyclones to meridional heat transport by the oceans. *J. Geophys. Res.* **106**, 14771–14781 (2001).

10. Knapp, K. R., Kruk, M. C., Levinson, D. H., Diamond, H. J. & Neumann, C. J. The International Best Track Archive for Climate Stewardship (IBTrACS): Unifying tropical cyclone data. *Bull. Amer. Meteor. Soc.* **91**, 363–376 (2010).
11. Hersbach, H. *et al.* The ERA5 global reanalysis. *Q. J. R. Meteorol. Soc.* **146**, 1999–2049 (2020).
12. Hu, K., Chan, J. C. L., Huang, G., Chen, G. & Mei, W. A train-like extreme multiple tropical cyclogenesis event in the Northwest Pacific in 2004. *Geophys. Res. Lett.* **45**, 8529–8535 (2018).
13. Mason, E., Pascual, A. & McWilliams, J. C. A New Sea Surface Height–Based Code for Oceanic Mesoscale Eddy Tracking. *Journal of Atmospheric and Oceanic Technology* **31**, 1181–1188 (2014).
14. Ma, Z., Fei, J., Liu, L., Huang, X. & Li, Y. An investigation of the influences of mesoscale ocean eddies on tropical cyclone intensities. *Mon. Weather Rev.* **145**, 1181–1201 (2017).
15. Mason, E., Pascual, A. & McWilliams, J. C. A new sea surface height–based code for oceanic mesoscale eddy tracking. *J. Atmos. Ocean. Technol.* **31**, 1181–1188 (2014).
16. Taburet, G. *et al.* DUACS DT2018: 25 years of reprocessed sea level altimetry products. *Ocean Sci.* **15**, 1207–1224 (2019).
17. Reagan, J. R. *et al.* World Ocean Atlas 2023. NOAA National Centers for Environmental Information <https://doi.org/10.25921/VA26-HV25> (2023).
18. Shang, X., Zhu, H., Chen, G., Xu, C. & Yang, Q. Research on cold core eddy

change and phytoplankton bloom induced by typhoons: Case studies in the South
China Sea. *Adv. Meteorol.* **2015**, 1–19 (2015).